

## RESULTS FROM PULSED NEUTRON SOURCE MEASUREMENTS IN THE YALINA-BOOSTER ADS EXPERIMENT

Carl-Magnus Persson<sup>1</sup>, Andrei Fokau<sup>1,2</sup>, Ivan Serafimovich<sup>2</sup>, Victor Bournos<sup>2</sup>, Yurii Fokov<sup>2</sup>, Christina Routkovskaia<sup>2</sup>, Hanna Kiyvitskaya<sup>2</sup>, Waclaw Gudowski<sup>1</sup>

<sup>1</sup>Royal Institute of Technology, Department of Reactor Physics: AlbaNova University Centre, SE-106 91, Stockholm, Sweden  
calleg@neutron.kth.se

<sup>2</sup>Joint Institute for Power and Nuclear Research: National Academy of Sciences of Belarus, Minsk, Sosny

*Two subcritical configurations of the zero-power coupled subcritical core YALINA-Booster have been identified through pulsed neutron source measurements. The area ratio and the slope fitting reactivity estimation methods have been utilized as well as the pulsed Rossi- $\alpha$  noise method. The measurements showed that despite the inhomogeneous two-zone core composition a clear single exponential prompt neutron decay was obtained. Spatial spread of the results and convergence issues related to the area ratio method are addressed.*

### I. YALINA-BOOSTER CORE LAYOUT

The YALINA-Booster is a subcritical core with two zones employing a fast and a thermal neutron spectrum respectively. The core consists of a central lead zone, a polyethylene zone, a radial graphite reflector and a front and back biological shielding consisting of borated polyethylene (Fig. 1). The loading is 132 fuel pins, containing 90% enriched metallic uranium, 563 fuel pins containing uranium dioxide of 36% enrichment and a maximum of 1141 EK-10 fuel pins containing uranium dioxide of 10% enrichment. The zero-power core is cooled by natural convection of the surrounding air.

The fast-spectrum lead zone and the thermal-spectrum polyethylene zone are separated by a so called thermal neutron filter, which consists of one layer of 108 metallic uranium pins and one layer of 116 boron carbide (B<sub>4</sub>C) pins, which are placed in the outermost two rows of the fast zone. Thermal neutrons diffusing from the thermal zone to the fast zone will either be absorbed by the boron or by the natural uranium, or they will be transformed into fast neutrons through fission in the natural uranium. In this way, a coupling of only fast neutrons between the two zones is maintained.

There are seven axial experimental channels (EC1B-EC4B and EC5T-EC7T) in the core and two axial experimental channels (EC8R and EC9R) and one radial experimental channel (EC10R) in the reflector. Moreover, there is one neutron flux monitoring channel in each

corner of the core. Three B<sub>4</sub>C-control rods, with a total reactivity worth of approximately -300 pcm can be inserted into the thermal zone. A detailed description of the core is available in the YALINA-Booster benchmark description<sup>1</sup>.

In these measurements, two configurations have been studied. These configurations have a fully loaded fast zone, as described above, and 1132 and 1061 fuel pins of 10% enrichment in the thermal zone respectively. The loading of these fuel pins was made based on cylindrical symmetry (Fig. 1).

### II. REACTIVITY DETERMINATION METHODS BASED ON A PULSED NEUTRON SOURCE

#### II.A. Area ratio and slope fitting

In this study, the area ratio method has been chosen as the reference method for reactivity estimations since it does not require calibration at delayed critical and that it has proven to be rather stable in other studies. By considering the fraction of prompt to delayed neutron areas in a PNS histogram, the reactivity in dollar can be obtained<sup>2</sup>:

$$\frac{\rho}{\beta_{eff}} = -\frac{A_p}{A_d}. \quad (1)$$

The prompt neutron area,  $A_p$ , and the delayed neutron area,  $A_d$ , are depicted in Fig. 2. If there is a non-negligible contribution from an inherent source, e.g. spontaneous fissions, it must be taken into account. However, in these measurements it was found that the inherent source was completely negligible.

If assuming that the point kinetic model is applicable, the reactivity can be determined from the prompt neutron decay constant,  $\alpha$ , if the effective delayed neutron fraction,  $\beta_{eff}$ , and the neutron reproduction time,  $\Lambda$ , are known<sup>3</sup>:

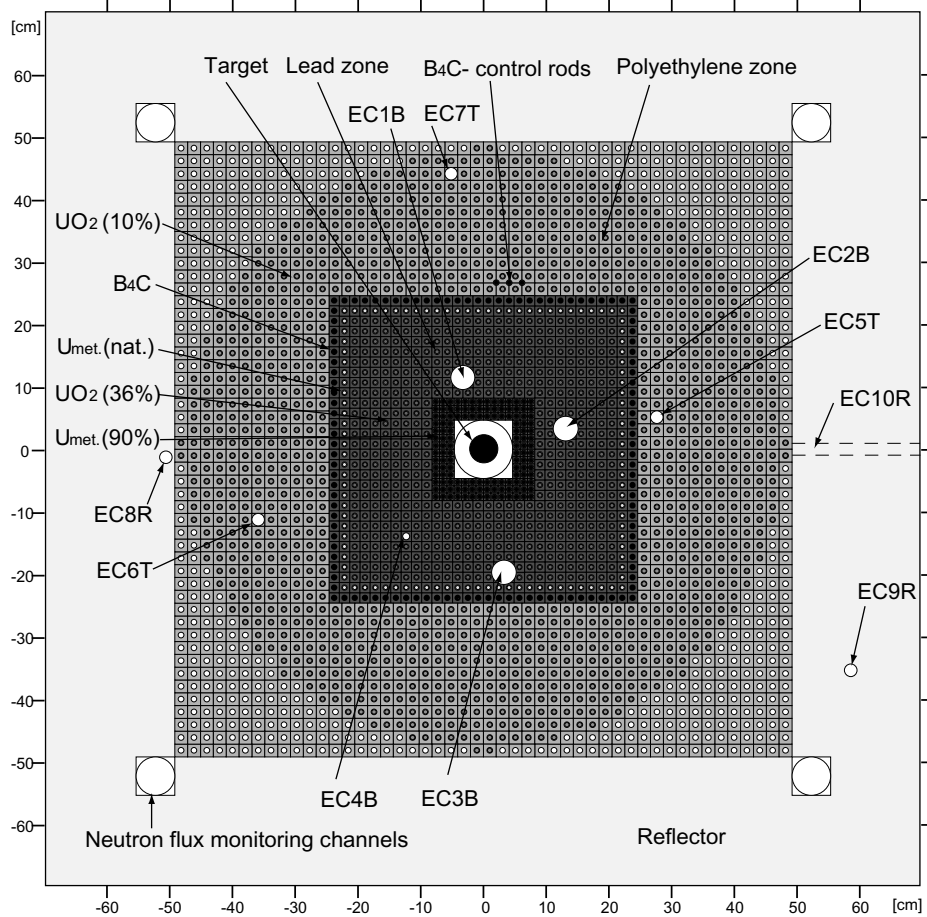


Fig. 1. Schematic cross-sectional view of YALINA-Booster (the 1132-configuration).

$$\alpha \equiv \frac{1}{n} \frac{dn}{dt} = \frac{\rho - \beta_{eff}}{\Lambda} \quad (2)$$

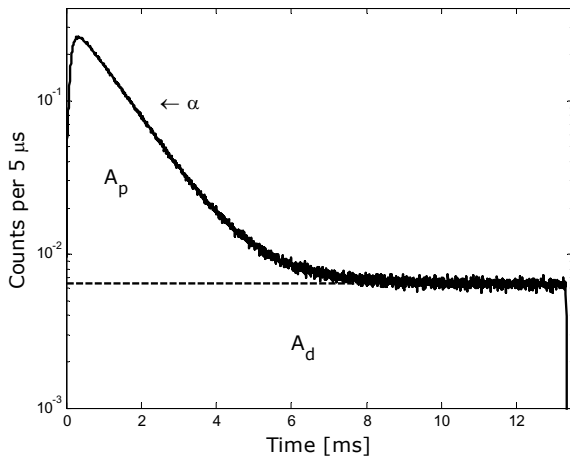


Fig. 2. Prompt and delayed neutron areas used in the area method, as well as the exponential decay of prompt neutrons (time discretization 5 μs).

## II.B. Pulsed Rossi- $\alpha$

The Rossi- $\alpha$  technique can be applied in the same way to data from a pulsed neutron source measurement as for a continuous source measurement. It has been shown that the pulsed Rossi- $\alpha$  histogram consists of three terms<sup>4</sup>:

$$p(t)dt = A_1 e^{\alpha t} dt + A_2 dt + A_3 \sum_{n=1}^{\infty} (a_n^2 + b_n^2) \cos(\omega_n t) dt \quad (3)$$

The first term is the ordinary correlated exponential term, also found in the classical formula for a steady state source, and the last two terms are uncorrelated terms. The last term is a non-decaying oscillating term consisting of a Fourier series representing the pulsed neutron source characteristics. The constants of Eq. (3) are given in Ref. [4]. Since the uncorrelated terms are non-decaying, the correlated term can be isolated by removing the contribution from the uncorrelated terms found at large  $t$ .

### III. EXPERIMENTAL RESULTS

#### III.A. Area ratio and slope fitting

PNS histograms for detectors in the core, EC6T, and the reflector, EC8R, are shown in Fig. 3 and Fig. 4. For comparison, histograms for both configurations in EC6T are shown in Fig. 5. The PNS histograms indicate a clear single exponential decay of the prompt neutron flux. The prompt neutron decay constants were found through non-linear fitting of a function of the form

$$f(t) = A_1 e^{\alpha t} + A_2. \quad (4)$$

The first transient part of each histogram was omitted and a sensibility analysis was performed to find the best starting point of the fitting. In all cases, a reduced  $\chi^2$ -value less than 1% from unity was obtained. Results for both configurations and for all experimental channels are shown in TABLE 1 and Fig. 6 indicating small spatial spreads of 1.1% and 1.5% respectively.

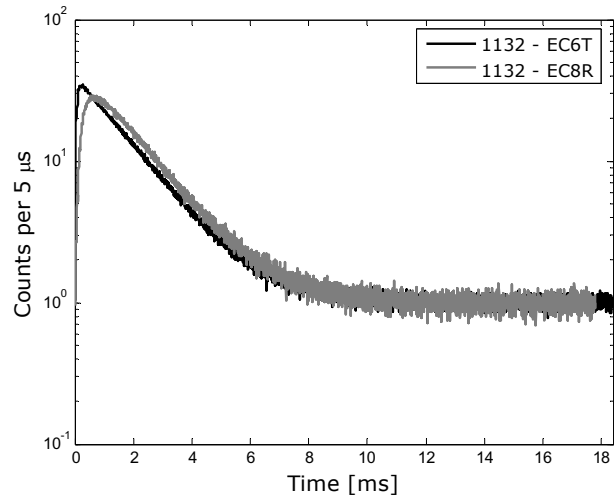


Fig. 3. PNS histogram for the 1132-configuration (normalized to the constant level and with time discretization 5  $\mu$ s).

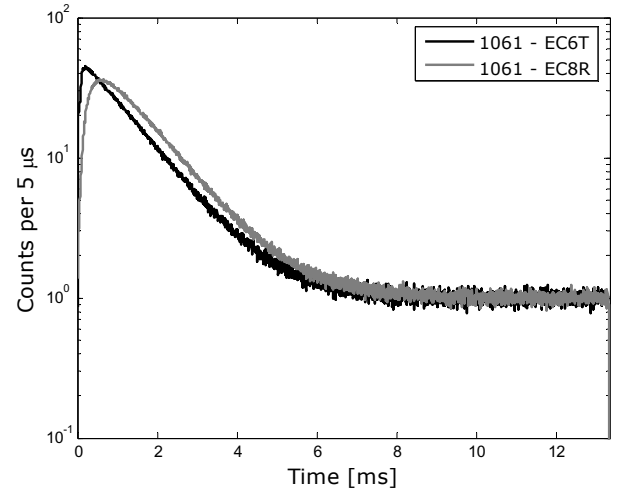


Fig. 4. PNS histogram for the 1061-configuration (normalized to the constant level and with time discretization 5  $\mu$ s).

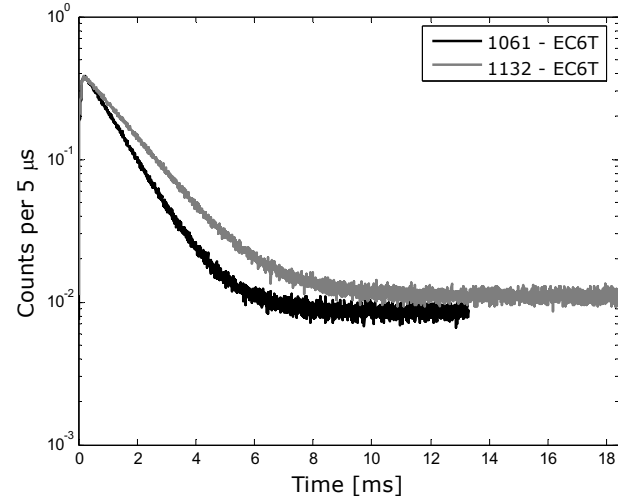


Fig. 5. PNS histogram for the central core channel, EC6T, for the 1061- and 1132-configurations (time discretization 5  $\mu$ s).

TABLE 1. Results from PNS measurements.

Conf.	EC	$\alpha$ [s <sup>-1</sup> ]	$\rho/\beta_{eff}$ [β]	$\Lambda/\beta_{eff}$ [ms]
1132	EC5T	-654.1±1.6	-3.60±0.03	7.04±0.04
	EC6T	-662.6±1.8	-3.36±0.02	6.58±0.04
	EC7T	-649.4±1.4	-3.37±0.02	6.73±0.03
	EC8R	-648.7±2.0	-3.61±0.02	7.11±0.03
	EC9R	-644.0±3.3	-3.92±0.03	7.65±0.05
Weighted mean value		-652.7	-3.54	6.96
Spread		7.1 (1.1%)	0.23 (6.5%)	0.42 (6.0%)
1061	EC5T	-875.0±1.9	-5.09±0.03	6.96±0.03
	EC6T	-892.1±2.7	-4.71±0.03	6.40±0.03
	EC7T	-866.7±2.2	-4.75±0.03	6.64±0.03
	EC8R	-863.4±3.2	-5.07±0.03	7.03±0.03
	EC9R	-860.1±3.6	-5.33±0.03	7.36±0.04
Weighted mean value		-872.7	-4.95	6.82
Spread		12.9 (1.5%)	0.26 (5.3%)	0.38 (5.5%)

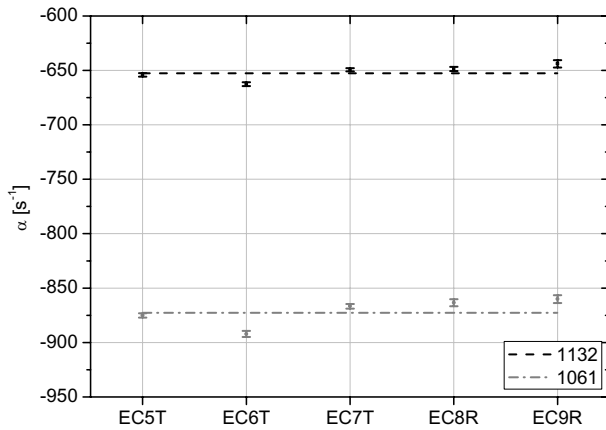


Fig. 6. Prompt neutron decay constants from the PNS fitting method for different detector positions. The weighted mean values are indicated as straight lines.

The constant level of delayed neutrons was found from the parameter  $A_2$  in Eq. (4). The results are shown in TABLE 1 and Fig. 7 and indicate a spatial spread of approximately 6% in the reactivity. An MCNP<sup>5</sup> analysis was performed based on the two nuclear data libraries JEFF3.1 and JENDL3.3. Results concerning  $k_{eff}$  and  $\beta_{eff}$  can be found in TABLE 2. In the analysis, the value  $\beta_{eff} = 733 \pm 21$  pcm has been used for both configurations. From the experimental values of the reactivities in dollars and the prompt neutron decay constants,  $k_{eff}$  and  $\Lambda$  have been calculated according to:

$$k_{eff} = \frac{1}{1 - \left[ \frac{\rho}{\beta_{eff}} \right]^{exp} \beta_{eff}^{MCNP}} \quad (5)$$

and

$$\Lambda = \frac{1}{\alpha^{exp}} \left( \left[ \frac{\rho}{\beta_{eff}} \right]^{exp} - 1 \right) \beta_{eff}^{MCNP}, \quad (6)$$

where “exp” refers to experimental data and “MCNP” to calculated values. Eq. (6) should be interpreted with caution since it relies on the assumption that the point kinetic approximation can be adopted. By using the weighted mean values and the spatial spread in the measured reactivities and prompt neutron decay constants, the following values are obtained:

$$k_{eff}^{1132} = 0.975 \pm 0.002$$

$$k_{eff}^{1061} = 0.965 \pm 0.002$$

$$\Lambda^{1132} = 51.0 \pm 3.4 \mu s$$

$$\Lambda^{1061} = 50.0 \pm 3.1 \mu s.$$

The values for  $k_{eff}$  are in good agreement with those from MCNP. There is only a small difference in neutron reproduction time for the two configurations.

From the measured reactivities, the reactivity difference can easily be calculated. According to Fig. 7, both configurations obey the same spatial dependence. Therefore, it is expected that the difference between the two reactivity levels has smaller spatial dependence. In fact, the spatial spread is small:  $\Delta\rho/\beta_{eff} = 1.41 \pm 0.05$  \$.

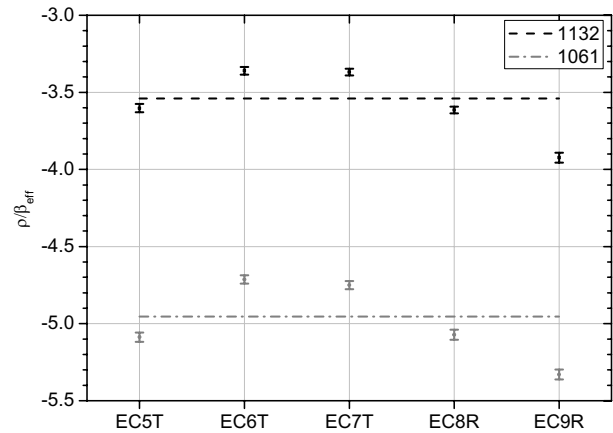


Fig. 7. Reactivity (in dollars) from the area method for different detector positions. The weighted mean values are indicated as straight lines.

TABLE 2. Results from MCNP.

Conf.	Library	$\beta_{eff}$ [pcm]	$k_{eff}$ (MCNP)
1132	JEFF3.1	734.6±6.5	0.97602±0.00004
	JENDL3.3	738.4±16	0.97646±0.00010
1061	JEFF3.1	728.2±8.9	0.96267±0.00005
	JENDL3.3	737.0±17	0.96343±0.00010

### III.A.1. Convergence of the area ratio estimator

Jammes et al have raised concerns that the conversion time of the area ratio reactivity estimator may not be sufficiently fast<sup>6</sup>. However, in these measurements, the deviation from the final result less than 1% was in general achieved within 10-15% of the total measurement time (Fig. 8). The pulsed source was operating for approximately five minutes before each measurement started, to make sure that a steady state delayed neutron precursor density had been accumulated.

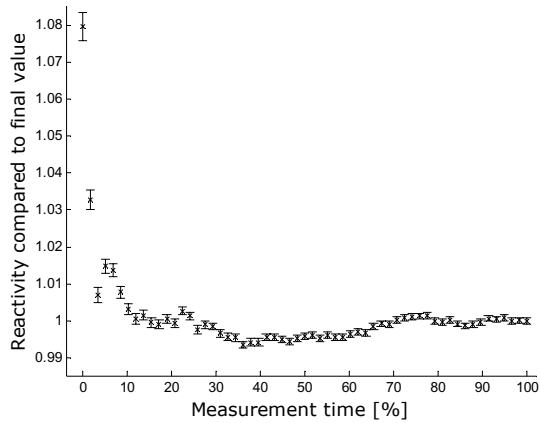


Fig. 8. Reactivity from the area ratio method as a function of measurement time.

### III.B. Pulsed Rossi- $\alpha$

Since the source is pulsed, the Rossi- $\alpha$  histogram looks very different from traditional Rossi- $\alpha$  histograms (Fig. 9). The assumption that the first term of Eq. (3) has decayed completely after 80 ms is made. At that time, the signal only consists of the two uncorrelated terms. Since these terms do not decay in time, experimental data can be chosen from the interval 80-93 ms (the last U-form) and then be deleted subsequently from the previous U-formed intervals. By doing so, only the correlated exponential term will be left, as depicted in Fig. 10. In an ideal case, the constant level after removal will be zero. Finally, the exponent is determined through the fitting of an exponential. An example of the final solution is depicted in Fig. 11.

All results are presented in TABLE 3. It is found that the results from the pulsed Rossi- $\alpha$  analysis are in general in agreement with the results from the PNS fitting method. The errors are larger for the Rossi- $\alpha$  case, due to the more complicated data treatment required to arrive at the result. A feature of the pulsed Rossi- $\alpha$  approach is that the correlated term is much higher compared to the traditional continuous source Rossi- $\alpha$  approach. Therefore it is expected that the pulsed method will give results with higher accuracy than the continuous source method.

TABLE 3. Results from the pulsed Rossi- $\alpha$  analysis.

Conf.	EC	$\alpha$ [s <sup>-1</sup> ]
1132	EC5T	-671±9
	EC9R	-618±44
1061	EC5T	-854±4
	EC6T	-881±9
	EC7T	-890±11
	EC9R	-842±36

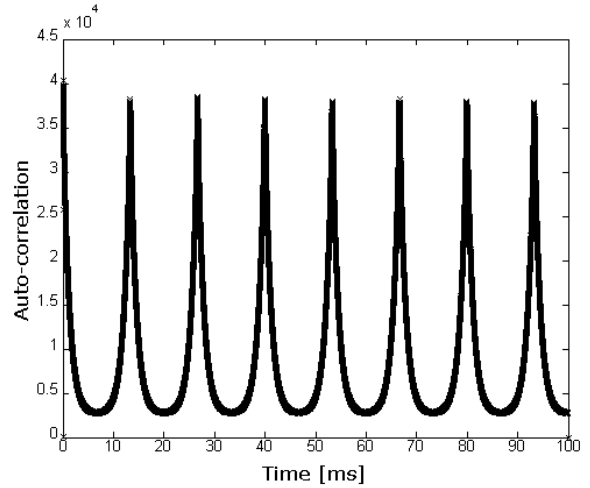


Fig. 9. Rossi- $\alpha$  histogram for YALINA-Booster with a pulsed source.

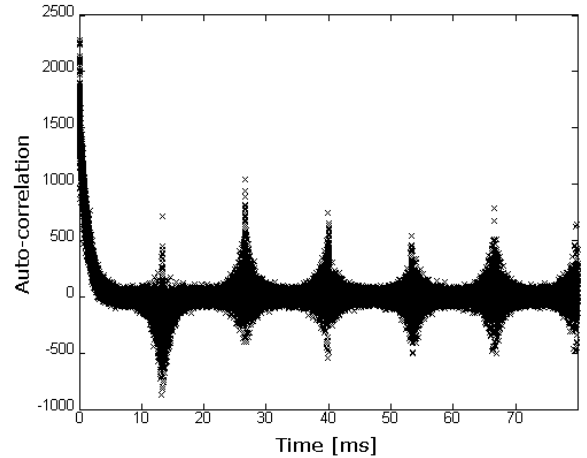


Fig. 10. Rossi- $\alpha$  histogram with the oscillation term removed.

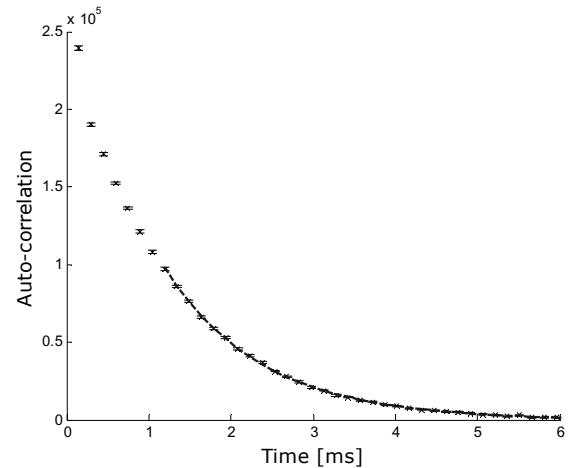


Fig. 11. Fitting of exponential to the Rossi- $\alpha$  histogram after the removal of the oscillation term.

#### IV. CONCLUSIONS

Two subcritical configurations of the YALINA-Booster experiment were characterized. It was found that the slope fitting technique gave results with small spatial spread, whereas the area ratio method gave results with a systematic spatial spread. Since the spatial spread in the reactivity was very similar for the studied configurations, the reactivity difference between the two configurations could be achieved with high accuracy. Moreover, it was shown that the area ratio method in these measurements converges rapidly to the final value. The pulsed Rossi- $\alpha$  method gave similar results as the slope fitting method but in a more time consuming and less straight forward way.

It is noticeable that although the core layout is complex, a very clear single exponential neutron pulse response was achieved.

#### ACKNOWLEDGMENTS

The construction of the YALINA-Booster facility has been done within the framework of the Belarus State Scientific Program "Instruments for Scientific Research". The work performed at KTH was financially supported by Svensk Kärnbränslehantering AB, SKB (the Swedish Nuclear Fuel and Waste Management Co). Financial support from the Swedish Institute making it possible to create scientific relation between Belarus and Sweden is cordially acknowledged.

The authors express their deepest gratitude to Filip Kondev, ANL, for sharing his experiences and for acting as an excellent interpreter during the experiments.

#### REFERENCES

1. H. Kiyavitskaya (coordinator), "YALINA-Booster Benchmark Specifications for the IAEA Coordinated Research Projects on Analytical and Experimental Benchmark Analysis on Accelerator Driven Systems and Low Enriched Uranium Fuel Utilization in Accelerator Driven Sub-Critical Assembly Systems", IAEA (2007).
2. N.G. Sjöstrand, "Measurement on a subcritical reactor using a pulsed neutron source", *Arkiv för fysik* 11, 13 (1956).
3. B.E. Simmons & J.S. King, "A Pulsed Technique for Reactivity Determination", *Nuclear Science and Engineering* 3, pp. 595-608 (1958).
4. Y. Kitamura et al., "Calculation of the stochastic pulsed Rossi-alpha formula and its experimental verification", *Progress in Nuclear Energy* 48, pp. 37-50, (2006).
5. X-5 Monte Carlo Team, "MCNP – A General Monte Carlo N-Particle Transport Code, Version 5", LA-UR-03-1987, Los Alamos National Laboratory, USA (2005).
6. C. Jammes et al., "On the Area Pulsed Neutron Source Technique Reactivity Estimator", *Int. Conf. on Accelerator Applications* (2005).